Research Square

Preprints are preliminary reports that have not undergone peer review.
They should not be considered conclusive, used to inform clinical practice,
or referenced by the media as validated information.

Selective Antiproliferative Activity of an Oleandrigenin-Derived Androstane in Prostate Cancer Cells

Martina Metz
Palacký University Olomouc
Jana Steigerová
jana.steigerova@upol.cz

Palacký University Olomouc
Marie Kvasnicová
Palacký University Olomouc
Zlata Rychnovská
Palacký University Olomouc
Tereza Kašparová
Palacký University Olomouc
Tereza Štenclová
Palacký University Olomouc
Lucie Rárová
Czech Academy of Sciences, Institute of Experimental Botany and Palacky University Olomouc
Karol Michalak
Polish Academy of Sciences
Jerzy Wicha
Polish Academy of Sciences
Miroslav Strnad
Czech Academy of Sciences, Institute of Experimental Botany and Palacky University Olomouc

Research Article

Keywords: Antiproliferative activity, Cardiac glycosides, Cell cycle, Prostate cancer, Steroid receptors

Posted Date: August 4th, 2026

DOI: https://doi.org/10.21203/rs.3.rs-10361917/v1

License: This work is licensed under a Creative Commons Attribution 4.0 International License.
Read Full License

Additional Declarations: No competing interests reported.

Abstract

Cardiac glycosides, traditionally used for heart failure, are increasingly recognized for their anticancer potential. This study evaluated the *in vitro* antitumor activity of ten cardiac glycoside derivatives on androgen-insensitive (DU-145) and androgen-sensitive (LNCaP) prostate cancer cells, utilizing non-tumorigenic RWPE-1 cells as a control. Key assays included cell viability, proliferation, cell cycle distribution, apoptosis, and nuclear steroid receptor analysis. Among the tested series, compound **10**, an oleandrigenin-derived androstane, exhibited the most significant therapeutic potential. It demonstrated pronounced effects on cell viability, proliferation, and apoptosis, while significantly altering molecular pathways and receptor dynamics specifically in prostate cancer cells. Crucially, compound **10** showed selective toxicity toward tumor cells with minimal impact on non-tumorigenic control; a distinct selectivity profile rarely observed in this class. These findings identify compound **10** as a promising candidate for novel prostate cancer therapies.

1. Introduction

Cardiac glycosides are a class of naturally occurring compounds traditionally used in the treatment of heart failure and arrhythmias due to their ability to inhibit Na^+/K^+-ATPase (NKA), a membrane protein essential for ionic homeostasis. Beyond its ion transport function, NKA also acts as a signal transducer involved in the regulation of cell proliferation and survival, making it an attractive target in cancer therapy (Ainembabazi et al., 2023; Castillo et al., 2011; L. Chen et al., 2019; Khajah et al., 2018). Recent studies, including our work on oleandrigenin-related androstane derivatives, further support the anticancer potential of this class of compounds (Bejček et al., 2021; Michalak et al., 2019, 2020). Structurally, cardiac glycosides consist of a steroid core linked to a sugar moiety at C-3 and a lactone ring at C-17β, and are classified into cardenolides and bufadienolides based on the lactone structure (El-Seedi et al., 2019; Melero et al., 2000; Winnicka et al., 2006). Structural modifications strongly influence both pharmacokinetic and pharmacodynamic properties. In our previous SAR analysis of oleandrigenin-related derivatives (**1**–**10**), we observed that 14β-hydroxy cardenolides exhibited high but non-selective cytotoxicity, whereas specific structural modifications conferred selectivity toward prostate cancer cells. Notably, the 14α,15α-epoxide derivative **10** showed improved tumor selectivity compared to its 14β,15β-isomer, highlighting the importance of stereochemistry in anticancer activity. Epidemiological and experimental evidence suggests that cardiac glycosides may reduce cancer incidence and inhibit tumor growth across multiple cancer types, including prostate cancer, where effects have been linked to Ca^{2+} dysregulation and apoptosis induction (Ishida et al., 2016; Karasneh et al., 2016; Platz et al., 2011; Yeh et al., 2003). Bufadienolides such as bufalin further demonstrate broad anticancer activity, including in prostate cancer models, through modulation of apoptotic signalling pathways and caspase activation (A. Chen et al., 2009; Li et al., 2009; Qi et al., 2011; Takai et al., 2008; Yu et al., 2008). Based on these observations, the present study aimed to evaluate the cytotoxic and molecular effects of cardiac glycoside and oleandrigenin-related derivatives (**1**–**10**) in prostate cancer models. We assessed their impact on cell viability, cell cycle progression, apoptosis, and steroid hormone receptor signaling. Experiments were performed in androgen-insensitive DU-145, androgen-sensitive LNCaP, and non-

tumorigenic RWPE-1 prostate cell lines. DU-145 cells lack androgen receptor (AR) expression and represent an aggressive, metastatic phenotype, whereas LNCaP cells are androgen-responsive and retain functional AR signaling. RWPE-1 cells served as a non-malignant control model for selectivity assessment (Sampson et al., 2013). Together, these models enabled evaluation of compound activity across different stages of prostate cancer progression and provided a basis for mechanistic studies focusing on androgen receptor signaling, cell cycle regulation, and apoptosis pathways.

2. Methods

2.1. Chemicals

The ten cardiac glycoside derivatives, as shown in Supplement Information (SI) Tab. S1 were tested in this study. These compounds were synthesized by our collaborators from the Polish Academy of Sciences in Warsaw, Poland. Detailed synthetic routes and characterization data for these compounds have been reported previously in the following articles (Michalak et al., 2019, 2020). These compounds include oleandrigenin (**1**) and its 3-*O*-acetyl derivative (**2**), 17β-(3-furyl)-oleandrigenin analogues (**3**–**5**), 3-*O*-methyl-5α-oleandrigenin (**6**) and the corresponding 14β,15β-epoxide (**9**). Seven of the derivatives are cardenolides **1**–**6** and **9**, while three compounds are oleandrigenin-related androstane derivatives **7**, **8** and **10**. The most promising compound regarding the selectivity of action 14α,15α-epoxide **10** has been subjected to detailed examination.

It should be noted that compounds **9** and **10** are isomers differing in orientation of the epoxide functional group – 14β,15β and 14α,15α, respectively. While cardenolides with 14β,15β epoxy-group are rather rare in natural sources, bufadienolides with that structural unit – cinobufagin and cinobufotalin were isolated from Chinese traditional antitumor drug Ch'an Su (Wei et al., 2019). The derivative **10**, with the 14α carbon – oxygen bond, formally does not belong to the class of cardenolides; its biological activity is presumably influenced by a combination of structural factors.

Compound purity was confirmed to be ≥ 98% via HPLC. Cardiac glycoside derivatives were dissolved in DMSO to yield 10 mM stock solutions, which were subsequently diluted in culture media to achieve the final concentrations. Structural formulas of all evaluated compounds are depicted in S) SI Fig. S1. Reagents were obtained as follows: the synthetic androgen R1881 (17β-hydroxy-17-methylestra-4,9,11-trien-3-on) from Perki-nElmer (Waltham, MA, USA), abiraterone from MedChemExpress (Monmouth Junction, NJ, USA), and galeterone from Sigma-Aldrich (St. Louis, MO, USA). Enzalutamide was generously provided by Dr. Frederic R. Santer (Innsbruck Medical University, Austria). Cell culture reagents and chemicals, including DMEM, RPMI 1640, fetal bovine serum (FBS), L-glutamine, recombinant human epidermal growth factor (EGF), bovine serum albumin (BSA), penicillin, streptomycin, 3-(4,5-dimethyltiazol-2-yl)-2,5-diphenyltetrazolium bromide (MTT), 4',6-diamidino-2-phenylindole (DAPI) were purchased from Sigma-Aldrich. Keratinocyte Serum-Free Medium (K-SFM) and B27 supplement without vitamin A, were sourced from Invitrogen (Waltham, MA, USA). Mowiol medium

was purchased from Calbiochem (Fremont, CA, USA). Primary and secondary antibodies are listed in SI Tab. S2.

2.2. Cell cultures

Human prostate cancer (DU-145, LNCaP) and noncancerous (RWPE-1) cell lines were obtained from the American Type Culture Collection (ATCC). The 22Rv1-ARE14 reporter cell line was generously provided by Prof. Zdeněk Dvořák (Palacký University, Czech Republic). RWPE-1 cells were maintained in K-SFM medium supplemented with bovine pituitary extract (BPE) and EGF. DU-145 cells were grown in DMEM, while both LNCaP and 22Rv1-ARE14 cells were cultured in RPMI 1640. All standard basal media were supplemented with 10% FBS, L-glutamine (250 mg/l), penicillin (100 U/ml), and streptomycin (100 mg/l). For specific assays requiring androgen deprivation, LNCaP and 22Rv1-ARE14 cells were cultivated in media supplemented with 2.5% or 10% charcoal-stripped serum (CSS), respectively. All cell cultures were maintained at 37°C in a humidified atmosphere containing 5% CO_2.

2.3. Cell viability test

Cells were seeded in 96-well plates (DU-145 and LNCaP: 5 × 10^3 cells/well; RWPE-1: 1 × 10^4 cells/well) and allowed to adhere for 24 or 48 h, respectively. At 70–80% confluence, cells were treated with test compounds (5–50 μM) for 48 h. Vehicle controls received an equivalent volume of DMSO. Cell viability and IC_{50} values were determined using the MTT assay. Absorbance was measured at 570 nm using a PowerWave XS microplate reader (BioTek Instruments, Agilent, USA). Cell viability was expressed relative to the vehicle control. IC_{50} values were calculated as the concentration reducing cell viability by 50%. Results are presented as mean ± SD from three independent experiments performed in triplicate.

2.4. Cell spheroid cultivation

96-well plates were covered with 1.5% agarose in DMEM medium, then seeded with cells (3.0 × 10^3 per well) grown in a spheroid medium (DMEM/F-12, 3:1, Invitrogen; 0.2× supplement B27 without vitamin A; 10 ng/ml EGF; 0.4% BSA) and after 24 h incubation, cells were treated with derivative **10** added to fresh medium at various concentrations (2–25 μM) up to 14 days. Spheroid growth was monitored throughout the incubation period, and images were captured on days 1, 7, and 14. On day 6 and 12, the culture medium was renewed with fresh medium supplemented with derivative **10**. The spheroids were examined and monitored to quantify the areas of the cell spheres. The effect of tested compound **10** was compared to untreated control spheroids using the ImageJ software (National Institutes of Health, Bethesda, MD, USA).

2.5. Flow cytometry

After trypsinization, DU-145 and LNCaP cells were seeded at defined densities into 60 mm dishes and treated with compound **10** at its IC_{50} concentration for 24/48 h, or with appropriate controls. Cells were then harvested, fixed in 70% ethanol, and stored at − 20°C. Before analysis, samples were stained with propidium iodide and RNase A, and cell cycle distribution was determined using a BD FACSVerse™ flow cytometer (BD Biosciences, CA, USA).

2.6. Western blot analysis

Cells were treated with compound **10** at its IC_{50} concentration for 24/48 h, R1881 (1 nM), enzalutamide (1 μM) or with appropriate controls (untreated or DMSO vehicle). Cell lysates were prepared by scraping and centrifugation (10,000 × g, 30 min, 4°C), and protein concentrations were determined using the Bradford assay (Bio-Rad, Hercules, CA, USA). Equal amounts of protein were separated by SDS-PAGE, transferred onto nitrocellulose membranes using a Trans-Blot SD semi-dry transfer cell (Bio-Rad), blocked with 5% non-fat dry milk in PBS containing 0.1% Tween-20 for 2 h, and incubated with primary antibodies overnight at 4°C, followed by HRP-conjugated secondary antibodies for 45 min. Protein bands were detected by enhanced chemiluminescence and visualized using the LI-COR Odyssey imaging system (Li-Cor Biotechnology, Lincoln, NE, USA). Band intensities from three independent experiments were quantified using the Gel Analysis tool in ImageJ, normalized to MCM-7 and β-actin, and expressed relative to untreated controls. All uncropped Western blot membranes are provided in Supplement Information.

2.7. TdT-Mediated dUTP nick end labelling (TUNEL) assay

Cells were seeded onto coverslips in 60 mm dishes at defined densities and treated with compound **10** at its IC_{50} concentration for 24/48 h. Cells were fixed in cold acetone–methanol (1:1) and processed using the In Situ Cell Death Detection Kit (Roche Diagnostics, Germany) according to the manufacturer's instructions. After DAPI counterstaining, samples were mounted in Mowiol and analysed using a BX50F fluorescence microscope (Olympus, Japan) to evaluate apoptotic morphology relative to vehicle controls.

2.8. Fluorescent immunocytochemical detection / Immunofluorescence labelling methods

Following the procedure described above, cells were incubated with primary antibodies against AR, pAR, ER-α, and ER-β for 90 min at room temperature. After washing with PBS, samples were incubated in the dark with fluorescently conjugated secondary antibodies. Samples were then mounted and processed according to the TUNEL protocol. Fluorescence images were acquired in TIFF format and channels were merged using ImageJ software

2.9. AR-transcriptional reporter assay

The AR-dependent reporter cell line 22Rv1-ARE14 was used to assess androgen receptor transcriptional activity. Cells were transfected with a reporter plasmid containing the androgen response element from the human PSA promoter (Bartonkova et al., 2015) and seeded in 96-well plates. After 24 h, the medium was replaced and cells were treated with the tested compounds (0.1–10 μM) or reference compounds (enzalutamide, galeterone, and abiraterone) in RPMI 1640 supplemented with charcoal-stripped serum (CSS) and 1 nM R1881. Untreated control cells received CSS alone. After 24 h incubation, cells were washed with PBS and lysed (10 mM Tris pH 7.4, 2 mM DTT, 1% Nonidet P40, 2 mM DCTA) for 10 min. Luciferin-based detection solution (20 mM tricine pH 7.8, 1.07 mM $MgSO_4 \cdot 7H_2O$, 5 mM ATP, 9.4 μM

luciferin) was added and luminescence was measured using a M200Pro microplate reader (Tecan, Austria). Results were normalized to cell viability.

2.10. Statistical analysis

All experiments were performed in independent triplicates. Data are presented as the mean ± standard deviation (SD). Statistical significance was determined using a Student's t-test in MS Excel 2019 (Microsoft) and GraphPad Prism 8 (GraphPad Software). A p-value of < 0.05 was considered statistically significant.

3. Results

3.1. Effects of cardiac glycosides on cell viability

Here, we present our results on the cytotoxicity of cardenolides **1**–**6** and **9**, as well as oleandrigenin – related androstane compounds **7**, **8** and **10**, determined by MTT assay on two human prostate cancer cell lines (hormone-independent DU-145 cells and hormone-dependent LNCaP cells) following 48 h of treatment. The cytotoxic effects on the cancer cells were compared with those observed in the non-cancerous RWPE-1 prostate cell line. The results are shown in Table 1. IC_{50} values were calculated from dose-response curves. Compounds **1** and **2** exhibited the highest cytotoxic among the cardiac glycosides tested, with IC_{50} values in the low micromolar range (0.5 μM) against LNCaP cells. However, these compounds also demonstrated increased cytotoxicity towards the normal prostate RWPE-1 cell line, resulting in a negative therapeutic window. Morphological changes in normal prostate and prostate cancer cells treated with compound **10** (IC_{50}) are shown in SI Fig S2.

Table 1
IC_{50} values (μM) obtained on two human prostate cancer cell lines (DU-145, LNCaP) and human normal prostate cells (RWPE-1) after 48 h of incubation with tested derivatives.

Cytotoxicity; IC_{50} (μM); 48 h			
Compound No.	DU-145	LNCaP	RWPE-1
1	< 0.5	< 0.5	< 0.5
2	< 0.5	0.8 ± 1.4	< 0.5
3	6.2 ± 0.6	14.2 ± 2.1	< 0.5
4	2.1 ± 1.5	4.4 ± 1.1	< 0.5
5	32.1 ± 1.9	10.3 ± 0.4	18.8 ± 2.5
6	10.1 ± 1.3	23.1 ± 0.4	2.6 ± 1.9
7	> 50	> 50	34.8 ± 1.8
8	> 50	> 50	21.2 ± 2.6
9	2.4 ± 2.2	5.2 ± 0.8	< 0.5
10	16.8 ± 0.3	18.0 ± 1.6	> 50

3.2. Effect of oleandrigenin-derived androstane derivative on the integrity of 3D prostate cancer spheroids

Improving the clinical success rate of new anticancer drugs requires better alignment between early discovery models, preclinical animal models, and patient-derived tumors. For solid tumors, this necessitates the implementation of three-dimensional (3D) *in vitro* models that accurately mimic the architecture and biology of human tissue. Recent advances in tissue engineering have facilitated the generation of 3D prostate cancer spheroids, providing a physiologically relevant platform for evaluating new therapeutic candidates.

Spheroids were generated by cultivating cell lines on an antiadhesive surface in the appropriate medium for 24 h, followed by treatment and observation for two weeks. The structural integrity of spheroids derived from the DU-145 and LNCaP cancer cell lines, as well as the non-cancerous human prostate cell line RWPE-1, was assessed after treatment with compound **10** at concentrations ranging from 2–25 μM for 1, 7 and 14 days. In the DU-145 cell line, a disruption of spheroid integrity and a loss of spheroids were observed in a concentration- and time-dependent manner. Significant changes in spheroid size compared to the untreated control cells were observed (Fig. 1). Despite this disruption, DU-145 cell spheroids exhibited greater resistance to compound **10** compared to LNCaP spheroids, with minimal changes in shape and size throughout the experiment, even at the highest concentrations. The effect of

compound **10** on LNCaP cell spheroids was more pronounced. The spheroids shrank and disintegrated progressively with increasing time and concentration. Significant changes in spheroid size were observed at concentrations of 10–25 μM ($p < 0.01$) as early as day 1 post-treatment compared to the control. By day 7, spheroid shrinkage and gradual disintegration were evident at these concentrations, and by day 14, decay of spheroids was observed at all tested concentrations. In contrast, compound **10** had no effect on non-tumorigenic RWPE-1 spheroids at any concentration or time point (Fig. 1). These findings are consistent with the cell viability results obtained from the MTT assay.

3.3. Effect of the cardiac glycoside derivative on cell cycle regulatory proteins

Given that compound **10** demonstrated a selective and significant inhibitory effect on prostate cancer cell growth, its impact on cell cycle progression and associated regulatory proteins was further investigated. In DU-145 cells, treatment with compound **10** increased the proportion of cells in the S phase, with a corresponding decrease in other phases at both 24 and 48 h (2A). In LNCaP cells, compound **10** induced G_1 phase arrest, accompanied by a reduction in the S and G_2/M populations at both time points (Fig. 2B).

Western blot analysis was performed to investigate whether the antiproliferative effects of the cardiac glycoside derivative **10** are mediated through alterations in cell cycle regulatory proteins (Fig. 3A). DU-145 and LNCaP cells were treated with compound **10** at IC_{50} concentrations for 24 and 48 h. Normalized protein expression levels relative to controls are shown in Fig. 3b (DU-145) and Fig. 3C (LNCaP). The CDK inhibitors $p16^{Ink4a}$ and $p21^{Waf1/Cip1}$ regulate cell cycle progression at the G_0/G_1 checkpoint, where their induction inhibits the G_1/S transition. Western blot analysis revealed upregulation of $p21^{Waf1/Cip1}$ in both cell lines after 24 h (2.0198 ± 0.27; $p < 0.05$) and 48 h (3.0354 ± 0.18; $p < 0.01$), with a more pronounced effect in LNCaP cells at 48 h. In contrast, p16Ink4a was downregulated after 24 h of treatment (0.4829 ± 0.05; $p < 0.01$). p53 plays a key role in cell cycle regulation and apoptosis. DU-145 cells, which harbor mutant p53, showed a decrease in p53 expression after 24 h (0.7420 ± 0.06; $p < 0.05$) and 48 h (0.2201 ± 0.02; $p < 0.001$) of treatment with compound **10**. In contrast, LNCaP cells, expressing wild-type p53, exhibited increased p53 levels at 24 h (3.2189 ± 0.18; $p < 0.01$) and a further increase at 48 h (5.7207 ± 0.77; $p < 0.05$). Retinoblastoma protein (Rb) is a key regulator of the cell cycle that prevents entry into S phase. CDK- and cyclin-mediated phosphorylation in late G_1 leads to Rb inactivation and release of E2F transcription factors, enabling cell cycle progression (van den Heuvel & Dyson, 2008). Rb protein was upregulated in both cell lines following treatment with compound **10** (DU-145, 24 h: 1.9418 ± 0.28; $p < 0.05$; LNCaP, 24 h: 3.9789 ± 0.55; $p < 0.05$; 48 h: 3.3138 ± 0.37; $p < 0.05$). Phosphorylated Rb (pRb) was increased in LNCaP cells after 48 h of treatment (7.6946 ± 1.10; $p < 0.05$). Src tyrosine kinase, implicated in castration-resistant prostate cancer progression and androgen receptor signaling (Gao et al., 2022), showed no changes in expression in either cell line. Cyclins A and B_1 were downregulated after 48 h in DU-145 cells and after 24 h in LNCaP cells (cyA: 0.5630 ± 0.05 vs. 0.6231 ± 0.07; cyB_1: 0.6380 ±

0.07 vs. 0.3328 ± 0.04; $p < 0.05 – 0.01$). No significant changes in cyclin D_1 were observed in DU-145 cells. Cyclin E was upregulated in both cell lines after 48 h of treatment (DU-145: 1.6427 ± 0.20; LNCaP: 1.6295 ± 0.19; $p < 0.05$). CDK4 expression decreased in DU-145 cells after 24 h (0.4175 ± 0.06; $p < 0.01$) but increased in LNCaP cells at 24 h (1.6787 0.16; $p < 0.05$) and 48 h (3.7800 ± 0.53; $p < 0.05$).

3.4. Induction of apoptotic pathways in prostate cancer cells

Changes in the expression of apoptosis-regulating proteins were assessed by Western blot analysis (Fig. 4a). DU-145 and LNCaP cells were treated with IC_{50} concentrations of compound **10** for 24 and 48 h and compared with untreated controls. As shown in Fig. 4A-C, the expression levels of the antiapoptotic proteins Bcl-2 and Bcl-X_L remained unchanged in both cell lines following treatment. Although the cleaved (15 kDa) fragment of the proapoptotic protein Bid was not detected, a significant reduction in full-length Bid (22 kDa) was observed in LNCaP cells after 24 h (0.2248 ± 0.02; $p < 0.001$) and 48 h (0.3049 ± 0.03; $p < 0.001$) of treatment with compound **10**. No changes in Bid expression were detected in DU-145 cells. Western blot analysis revealed downregulation of caspase-3 in DU-145 cells after 24 h (0.2896 ± 0.05; $p < 0.01$), whereas cleaved caspase-3 was detected in both cell lines after 48 h, indicating activation of apoptotic pathways. Apoptosis was further confirmed by TUNEL assay (Fig. 4D), which demonstrated a significant increase in apoptotic cells in both DU-145 and LNCaP cells following treatment with compound **10** at IC_{50} concentrations. Notably, LNCaP cells exhibited a higher proportion of apoptotic cells after 48 h compared with DU-145 cells.

3.5. Expression and localization of androgen and estrogen receptors after cardiac glycoside treatment

To investigate the effects of compound **10** on steroid hormone receptor expression and subcellular localization in prostate cancer cell lines, Western blotting was used to assess receptor expression, whereas immunofluorescence was employed to examine receptor localization following treatment (Fig. 5). Western blot analysis (Fig. 5A, B) revealed that AR protein was detected in LNCaP cells, whereas no AR signal was observed in DU-145 cells. In LNCaP cells, AR protein levels were reduced after 24 (0.6212 ± 0.07; $p < 0.05$) and 48 h (0.6843 ± 0.09; $p < 0.05$) of treatment. ER-α protein levels decreased (0.6386 ± 0.04; $p < 0.01$) after 48 h of treatment in DU-145 cells, while an increase in ER-α protein levels (1.8979 ± 0.17; $p > 0.05$) was observed after 48 h of treatment in LNCaP cells. ER-β protein levels increased in both cell lines, with elevated levels detected after 24 h of treatment in DU-145 cells (2.0684 ± 0.21; $p < 0.05$) and after 24 h of treatment in LNCaP cells (1.3604 ± 0.12; $p > 0.05$). Immunofluorescence analysis (Fig. 5D) revealed low levels of ER-α, predominantly localized in the nucleus, with no detectable changes following treatment. ER-β was detected in both the nucleus and cytoplasm of control cells and its expression and localization remained unchanged after exposure to compound **10**. In LNCaP cells (Fig. 5D), AR was localized in both the nucleus and cytoplasm under control conditions. Treatment with compound **10** reduced AR expression in both compartments. ER-α

was detected in both nuclear and cytoplasmic compartments and was not affected by treatment. ER-β showed a perinuclear cytoplasmic localization in control cells, whereas treatment resulted in increased cytoplasmic accumulation.

Western blot analysis was performed to further evaluate the effects of compound **10** on steroid receptor expression and AR-related signalling (Fig. 6). In LNCaP cells, compound **10** modulated AR signaling, as reflected by changes in AR-regulated proteins when compared with cells treated with the androgen agonist R1881 and the antagonist enzalutamide. A significant downregulation of phosphorylated AR (pAR Ser81) (0.2666 ± 0.04; $p < 0.01$), PSA (0.7775 ± 0.06; $p < 0.05$), and Nkx3.1 (0.7132 ± 0.05; $p < 0.05$) was observed after 24 h of treatment (Fig. 6A, B). The effect of compound **10** was more pronounced than that of enzalutamide alone. Consistent with immunofluorescence data (Fig. 6C), AR protein expression was reduced after 24 h of exposure to compound **10** (0.7084 ± 0.07; $p < 0.05$). Moreover, combined treatment with compound **10** and enzalutamide further decreased AR expression (0.5570 ± 0.05; $p < 0.01$), whereas enzalutamide alone induced an increase in AR levels (1.7736 ± 0.12; $p < 0.05$) (Fig. 6). A similar trend was observed for pAR (Fig. 6A, B). These findings were supported by immunofluorescence analysis, which revealed treatment-dependent alterations in AR and pAR localization (Fig. 6C). Co-treatment with compound **10** and enzalutamide reduced both cytoplasmic and nuclear AR signal intensity, accompanied by decreased nuclear pAR staining. In contrast, R1881 stimulation increased AR and pAR signal intensity, while co-treatment with compound **10** attenuated this response compared with R1881 alone.

3.6. Effect of cardiac glycosides derivatives on androgen receptor transcriptional activity

To evaluate the effects of the synthesized cardenolides and oleandrigenin-derived androstane derivatives on AR signaling, AR-mediated transcription was assessed in the 22Rv1-ARE14 reporter cell line. All compounds inhibited AR transcriptional activity in a dose-dependent manner (Fig. 7). At 10 μM, compounds **1**–**5** and **8**–**10** showed greater inhibitory activity than galeterone, while all tested derivatives were more effective than abiraterone. Enzalutamide was less effective than compounds **1**, **2**, **4**, and **9** at concentrations of 2.5, 5 and 10 μM. Among the tested derivatives, compounds **1**, **2**, and **9** produced the strongest inhibition of AR-mediated transcription at 10 μM.

4. Discussion

Prostate cancer remains a leading malignancy in men, and although androgen deprivation therapy is effective in early stages, progression to androgen-independent disease represents a major clinical challenge (Rebello et al., 2021). This underscores the need for novel compounds targeting multiple cellular pathways. In this study, newly synthesized oleandrigenin-related androstane derivatives were evaluated in androgen-sensitive (LNCaP), androgen-insensitive (DU-145), and non-cancerous (RWPE-1) prostate cell models. DU-145 cells showed slightly higher sensitivity than LNCaP, likely reflecting their faster proliferation and distinct genetic background. Structure–activity relationship analysis revealed

that cardenolides were highly cytotoxic but non-selective, whereas structural modification at the 14α,15α-position (compound **10**) resulted in improved tumor selectivity, supporting its selection for mechanistic studies. Cardiac glycosides, including oleandrin and *Nerium oleander* extracts, exert anticancer effects through inhibition of Na^+/K^+-ATPase and downstream signaling pathways, including regulation of fibroblast growth factor-2 (FGF-2) export regulation (Pathak et al., 2000; Smith et al., 2001). These mechanisms may also contribute to the strong activity of our derivatives, consistent with previous findings on cardenolide-based compounds (Michalak et al., 2019, 2020). However, sensitivity to cardiac glycosides varies across prostate cancer models, with LNCaP cells often showing higher responsiveness than PC-3 or DU-145 in other studies (Rascón-Valenzuela et al., 2015; Ye et al., 2024; Yeh et al., 2003).

Importantly, compound **10** also demonstrated significant activity in 3D spheroid models, where LNCaP spheroids were markedly more sensitive than DU-145, while RWPE-1 spheroids remained unaffected. These results align with reports that 3D cultures exhibit altered drug responses due to diffusion limitations, hypoxic gradients, and increased cell-cell interactions (Chao et al., 2017; Gong et al., 2015; Hickman et al., 2014; Nath & Devi, 2016; Thoma et al., 2014), highlighting the relevance of physiologically more complex models.

Early genetic changes associated with tumorigenesis often involved genes responsible for cell cycle regulation. These changes frequently lead to the loss of the G_1 checkpoint and disruption of the cell cycle in cancer cells (Lomazzi et al., 2002). At the molecular level, compound **10** induced cell cycle perturbation in both models, characterized by S-phase accumulation in DU-145 cells and G_0/G_1 arrest in LNCaP cells. These effects were accompanied by deregulation of key regulators including p21, p53, Rb, cyclins, and CDKs, indicating disruption of both G_1/S and G_2/M transitions. These results suggest that compound **10** may modulate cell cycle progression through a p53/p21-dependent G_1 checkpoint in LNCaP cells, whereas in DU-145 cells it may affect S-phase progression in a p53-independent manner. Changes in Rb phosphorylation and cyclin expression likely reflect downstream and compensatory responses rather than a single linear signaling cascade. Similar modulation of cell cycle regulators has been reported for other cardiac glycosides, including bufalin and related compounds (Chang et al., 2018; Kaushik et al., 2017; W.-J. Leu et al., 2014; Takai et al., 2008; Zhang et al., 2018). Furthermore, compound **10** triggered apoptotic signaling, as evidenced by increased TUNEL positivity, particularly in LNCaP cells. While anti-apoptotic Bcl-2 family proteins remained largely unchanged, alterations in Bid processing and caspase-3 activation suggest involvement of the intrinsic apoptotic pathway. These findings are consistent with previous reports on cardiac glycoside-induced apoptosis in cancer cells (W. Leu et al., 2020; Wu et al., 2017; Yeh et al., 2003).

Finally, compound **10** modulated AR signaling at multiple levels. In LNCaP cells, AR expression and nuclear localization were reduced, accompanied by suppression of AR-regulated targets, including PSA, Nkx3.1, and pAR. These effects were comparable to enzalutamide, indicating a strong functional impact on AR signaling. Additionally, immunofluorescence analysis showed altered AR and pAR localization after compound **10** treatment. Compound **10** reduced the R1881-induced increase in AR and pAR signals, indicating modulation of androgen-dependent AR signaling.

Consistently, compound **10** markedly attenuated AR transcriptional activity in 22Rv1-ARE14 reporter assays under androgen-stimulated conditions. Importantly, ER-α and ER-β expression remained largely unchanged, suggesting selective targeting of AR-driven pathways. Similar AR suppression has been reported for bufalin and other cardiac glycosides in prostate cancer models, supporting a conserved mechanism of steroid receptor modulation within this compound class (Yu et al., 2008; Zhang et al., 2018).

Overall, compound **10** exerts multitarget anticancer effects involving cell cycle arrest, apoptosis induction, and modulation of androgen receptor signaling, supporting its potential as a lead structure for further development in prostate cancer therapy.

5. Conclusion

Cardiac glycoside derivatives were evaluated for their antitumor activity in prostate cancer cell lines, with compound **10** identified as the most potent and selective agent. It was further characterized in 2D and 3D models, where it affected cell viability, cell cycle progression, apoptosis, and androgen receptor signalling in a cell line–dependent manner. DU-145 cells showed S-phase accumulation, whereas LNCaP cells exhibited G_0/G_1 arrest and increased apoptosis. In contrast, modulation of steroid receptor signalling was more pronounced in LNCaP cells, while DU-145 cells were less responsive at the receptor level. These findings suggest that compound **10** exerts its effects through multiple cellular pathways, including cell cycle regulation, apoptosis induction, and modulation of AR-associated signalling. However, the exact molecular targets remain to be fully elucidated. Further *in vivo* validation and mechanistic studies will be necessary to confirm its therapeutic potential. Overall, this study supports cardiac glycosides as promising scaffolds for the development of novel prostate cancer therapeutics.

Declarations

Acknowledgements

We thank Monika Levková, Jana Hrubešová, Eva Pimrová, and Anežka Šindlerová for their excellent technical assistance with the experiments. The authors thank prof. Zdenek Dvorak for the kind gift of 22Rv1-ARE14 cells.

Author contributions

M.M.: Writing – review & editing, Writing – original draft, Methodology, Investigation, Formal analysis, Data curation, Conceptualization. J.S.: Writing – review & editing, Supervision, Project administration. M.K.: Methodology, Investigation. Z.R.: Methodology, Investigation. T.K.: Methodology, Investigation. T.Š.: Methodology, Investigation. L.R.: Data curation, Conceptualization. K.M.: Conceptualization, Formal analysis. J.W.: Project administration, Writing – review & editing. M.S.: Project administration, Writing – review & editing.

Funding

The work was supported by the European Union - Next Generation EU (Project National Institute for Cancer Research, Programme EXCELES, Project No. LX22NPO5102) and by grants 23-05474S from the Grant Agency of the Czech Republic, LF_2025_001 from Palacký University, and DRO 61989592 from the Czech Ministry of Education, Youth and Sports.

Declaration of competing interest

The authors declare that they have no known competing financial interests or personal relationships that could have appeared to influence the work reported in this paper.

Data availability

All data generated or analysed during this study are included in this published article.

Declaration of interests

The authors have no relevant financial or non-financial interests to disclose.

Ethics statement

We confirm that this manuscript has not been published previously and is not under consideration by any other journal. All authors have approved the manuscript and agree with its submission to *Cell Biology and Toxicology*.

References

1. Ainembabazi, D., Zhang, Y., & Turchi, J. J. (2023). The mechanistic role of cardiac glycosides in DNA damage response and repair signaling. *Cellular and Molecular Life Sciences*, *80*(9), 250–250. https://doi.org/10.1007/s00018-023-04910-9
2. Bartonkova, I., Novotna, A., & Dvorak, Z. (2015). Novel Stably Transfected Human Reporter Cell Line AIZ-AR as a Tool for an Assessment of Human Androgen Receptor Transcriptional Activity. *PLOS ONE*, *10*(3), e0121316–e0121316. https://doi.org/10.1371/journal.pone.0121316
3. Bejček, J., Spiwok, V., Kmoníčková, E., & Rimpelová, S. (2021). Na+/K+-ATPase Revisited: On Its Mechanism of Action, Role in Cancer, and Activity Modulation. *Molecules*, *26*(7), 1905–1905. https://doi.org/10.3390/molecules26071905
4. Castillo, J. P., De Giorgis, D., Basilio, D., Gadsby, D. C., Rosenthal, J. J. C., Latorre, R., Holmgren, M., & Bezanilla, F. (2011). Energy landscape of the reactions governing the Na + deeply occluded state of the Na + /K + -ATPase in the giant axon of the Humboldt squid. *Proceedings of the National Academy of Sciences*, *108*(51), 20556–20561. https://doi.org/10.1073/pnas.1116439108
5. Chang, H., Li, J., Cao, Y., Liu, T., Shi, S., & Chen, W. (2018). Bufadienolides from Venenum Bufonis Inhibit mTOR-Mediated Cyclin D1 and Retinoblastoma Protein Leading to Arrest of Cell Cycle in

Cancer Cells. *Evidence-Based Complementary and Alternative Medicine*, *2018*(1). https://doi.org/10.1155/2018/3247402

6. Chao, M.-W., Chen, T.-H., Huang, H.-L., Chang, Y.-W., HuangFu, W.-C., Lee, Y.-C., Teng, C.-M., & Pan, S.-L. (2017). Lanatoside C, a cardiac glycoside, acts through protein kinase Cδ to cause apoptosis of human hepatocellular carcinoma cells. *Scientific Reports*, *7*(1), 46134–46134. https://doi.org/10.1038/srep46134
7. Chen, A., Yu, J., Zhang, L., Sun, Y., Zhang, Y., Guo, H., Zhou, Y., Mitchelson, K., & Cheng, J. (2009). Microarray and biochemical analysis of bufalin-induced apoptosis of HL-60 Cells. *Biotechnology Letters*, *31*(4), 487–494. https://doi.org/10.1007/s10529-008-9888-x
8. Chen, L., Jiang, P., Li, J., Xie, Z., Xu, Y., Qu, W., Feng, F., & Liu, W. (2019). Periplocin promotes wound healing through the activation of Src/ERK and PI3K/Akt pathways mediated by Na/K-ATPase. *Phytomedicine*, *57*, 72–83. https://doi.org/10.1016/j.phymed.2018.12.015
9. El-Seedi, H. R., Khalifa, S. A. M., Taher, E. A., Farag, M. A., Saeed, A., Gamal, M., Hegazy, M.-E. F., Youssef, D., Musharraf, S. G., Alajlani, M. M., Xiao, J., & Efferth, T. (2019). Cardenolides: Insights from chemical structure and pharmacological utility. *Pharmacological Research*, *141*, 123–175. https://doi.org/10.1016/j.phrs.2018.12.015
10. Gao, L., Han, B., & Dong, X. (2022). The Androgen Receptor and Its Crosstalk With the Src Kinase During Castrate-Resistant Prostate Cancer Progression. *Frontiers in Oncology*, *12*. https://doi.org/10.3389/fonc.2022.905398
11. Gong, X., Lin, C., Cheng, J., Su, J., Zhao, H., Liu, T., Wen, X., & Zhao, P. (2015). Generation of Multicellular Tumor Spheroids with Microwell-Based Agarose Scaffolds for Drug Testing. *PLOS ONE*, *10*(6), e0130348–e0130348. https://doi.org/10.1371/journal.pone.0130348
12. Hickman, J. A., Graeser, R., de Hoogt, R., Vidic, S., Brito, C., Gutekunst, M., van der Kuip, H., & IMI PREDECT consortium. (2014). Three-dimensional models of cancer for pharmacology and cancer cell biology: Capturing tumor complexity in vitro/ex vivo. *Biotechnology Journal*, *9*(9), 1115–1128. https://doi.org/10.1002/biot.201300492
13. Ishida, J., Konishi, M., Ebner, N., & Springer, J. (2016). Repurposing of approved cardiovascular drugs. *Journal of Translational Medicine*, *14*(1), 269–269. https://doi.org/10.1186/s12967-016-1031-5
14. Karasneh, R. A., Murray, L. J., Hughes, C. M., & Cardwell, C. R. (2016). Digoxin use after diagnosis of prostate cancer and survival: A population-based cohort study. *Pharmacoepidemiology and Drug Safety*, *25*(9), 1099–1103. https://doi.org/10.1002/pds.4018
15. Kaushik, V., Yakisich, J. S., Azad, N., Kulkarni, Y., Venkatadri, R., Wright, C., Rojanasakul, Y., & Iyer, A. K. V. (2017). Anti-Tumor Effects of Cardiac Glycosides on Human Lung Cancer Cells and Lung Tumorspheres. *Journal of Cellular Physiology*, *232*(9), 2497–2507. https://doi.org/10.1002/jcp.25611
16. Khajah, M. A., Mathew, P. M., & Luqmani, Y. A. (2018). Na+/K+ ATPase activity promotes invasion of endocrine resistant breast cancer cells. *PLOS ONE*, *13*(3), e0193779–e0193779.

https://doi.org/10.1371/journal.pone.0193779

17. Leu, W., Wang, C., Hsu, J., Chen, I., Chang, H., & Guh, J. (2020). Ascleposide, a natural cardenolide, induces anticancer signaling in human castration-resistant prostatic cancer through Na + /K + -ATPase internalization and tubulin acetylation. *The Prostate*, *80*(4), 305–318. https://doi.org/10.1002/pros.23944
18. Leu, W.-J., Chang, H.-S., Chan, S.-H., Hsu, J.-L., Yu, C.-C., Hsu, L.-C., Chen, I.-S., & Guh, J.-H. (2014). Reevesioside A, a Cardenolide Glycoside, Induces Anticancer Activity against Human Hormone-Refractory Prostate Cancers through Suppression of c-myc Expression and Induction of G1 Arrest of the Cell Cycle. *PLoS ONE*, *9*(1), e87323–e87323. https://doi.org/10.1371/journal.pone.0087323
19. Li, D., Qu, X., Hou, K., Zhang, Y., Dong, Q., Teng, Y., Zhang, J., & Liu, Y. (2009). PI3K/Akt is involved in bufalin-induced apoptosis in gastric cancer cells. *Anti-Cancer Drugs*, *20*(1), 59–64. https://doi.org/10.1097/CAD.0b013e3283160fd6
20. Lomazzi, M., Moroni, M. C., Jensen, M. R., Frittoli, E., & Helin, K. (2002). Suppression of the p53- or pRB-mediated G1 checkpoint is required for E2F-induced S-phase entry. *Nature Genetics*, *31*(2), 190–194. https://doi.org/10.1038/ng891
21. Melero, C. P., Medarde, M., & San Feliciano, A. (2000). A Short Review on Cardiotonic Steroids and Their Aminoguanidine Analogues. *Molecules*, *5*(1), 51–81. https://doi.org/10.3390/50100051
22. Michalak, K., Rárová, L., Kubala, M., Čechová, P., Strnad, M., & Wicha, J. (2019). Synthesis and evaluation of cytotoxic and Na+/K+-ATP-ase inhibitory activity of selected 5α-oleandrigenin derivatives. *European Journal of Medicinal Chemistry*, *180*, 417–429. https://doi.org/10.1016/j.ejmech.2019.07.028
23. Michalak, K., Rárová, L., Kubala, M., Štenclová, T., Strnad, M., & Wicha, J. (2020). Synthesis and evaluation of Na+/K+-ATP-ase inhibiting and cytotoxic in vitro activities of oleandrigenin and its selected 17β-(butenolidyl)- and 17β-(3-furyl)- analogues. *European Journal of Medicinal Chemistry*, *202*, 112520–112520. https://doi.org/10.1016/j.ejmech.2020.112520
24. Nath, S., & Devi, G. R. (2016). Three-dimensional culture systems in cancer research: Focus on tumor spheroid model. *Pharmacology & Therapeutics*, *163*, 94–108. https://doi.org/10.1016/j.pharmthera.2016.03.013
25. Pathak, S., Multani, A. S., Narayan, S., Kumar, V., & Newman, R. A. (2000). AnvirzelTM, an extract of Nerium oleander, induces cell death in human but not murine cancer cells. *Anti-Cancer Drugs*, *11*(6), 455–463. https://doi.org/10.1097/00001813-200007000-00006
26. Platz, E. A., Yegnasubramanian, S., Liu, J. O., Chong, C. R., Shim, J. S., Kenfield, S. A., Stampfer, M. J., Willett, W. C., Giovannucci, E., & Nelson, W. G. (2011). A Novel Two-Stage, Transdisciplinary Study Identifies Digoxin as a Possible Drug for Prostate Cancer Treatment. *Cancer Discovery*, *1*(1), 68–77. https://doi.org/10.1158/2159-8274.CD-10-0020
27. Qi, F., Inagaki, Y., Gao, B., Cui, X., Xu, H., Kokudo, N., Li, A., & Tang, W. (2011). Bufalin and cinobufagin induce apoptosis of human hepatocellular carcinoma cells via Fas- and mitochondria-mediated pathways. *Cancer Science*, *102*(5), 951–958. https://doi.org/10.1111/j.1349-7006.2011.01900.x

28. Rascón-Valenzuela, L., Velázquez, C., Garibay-Escobar, A., Medina-Juárez, L. A., Vilegas, W., & Robles-Zepeda, R. E. (2015). Antiproliferative activity of cardenolide glycosides from Asclepias subulata. *Journal of Ethnopharmacology*, *171*, 280–286. https://doi.org/10.1016/j.jep.2015.05.057
29. Rebello, R. J., Oing, C., Knudsen, K. E., Loeb, S., Johnson, D. C., Reiter, R. E., Gillessen, S., Van der Kwast, T., & Bristow, R. G. (2021). Prostate cancer. *Nature Reviews Disease Primers*, *7*(1), 9–9. https://doi.org/10.1038/s41572-020-00243-0
30. Sampson, N., Neuwirt, H., Puhr, M., Klocker, H., & Eder, I. E. (2013). In vitro model systems to study androgen receptor signaling in prostate cancer. *Endocrine-Related Cancer*, *20*(2), R49–R64. https://doi.org/10.1530/ERC-12-0401
31. Smith, J. A., Madden, T., Vijjeswarapu, M., & Newman, R. A. (2001). Inhibition of export of fibroblast growth factor-2 (FGF-2) from the prostate cancer cell lines PC3 and DU145 by anvirzel and its cardiac glycoside component, oleandrin11Abbreviations: PARP, poly(ADP-ribose) polymerase; NF-κB, nuclear factor-κB; FGF-2, fibroblast growth factor-2; ER, endoplasmic reticulum; and MTT, 3-(4,5-dimethylthiazol-2-yl)-2,5-diphenyltetrazolium bromide. *Biochemical Pharmacology*, *62*(4), 469–472. https://doi.org/10.1016/S0006-2952(01)00690-6
32. Takai, N., Ueda, T., Nishida, M., Nasu, K., & Narahara, H. (2008). Bufalin induces growth inhibition, cell cycle arrest and apoptosis in human endometrial and ovarian cancer cells. *International Journal of Molecular Medicine*, *21*(5), 637–643.
33. Thoma, C. R., Zimmermann, M., Agarkova, I., Kelm, J. M., & Krek, W. (2014). 3D cell culture systems modeling tumor growth determinants in cancer target discovery. *Advanced Drug Delivery Reviews*, *69–70*, 29–41. https://doi.org/10.1016/j.addr.2014.03.001
34. van den Heuvel, S., & Dyson, N. J. (2008). Conserved functions of the pRB and E2F families. *Nature Reviews Molecular Cell Biology*, *9*(9), 713–724. https://doi.org/10.1038/nrm2469
35. Wei, W.-L., Hou, J.-J., Wang, X., Yu, Y., Li, H.-J., Li, Z.-W., Feng, Z.-J., Qu, H., Wu, W.-Y., & Guo, D.-A. (2019). Venenum bufonis: An overview of its traditional use, natural product chemistry, pharmacology, pharmacokinetics and toxicology. *Journal of Ethnopharmacology*, *237*, 215–235. https://doi.org/10.1016/j.jep.2019.03.042
36. Winnicka, K., Bielawski, K., & Bielawska, A. (2006). Cardiac glycosides in cancer research and cancer therapy. *Acta Poloniae Pharmaceutica*, *63*(2), 109–115.
37. Wu, S., Bau, D., Hsiao, Y., Lu, K., Hsia, T., Lien, J., Ko, Y., Hsu, W., Yang, S., Huang, Y., & Chung, J. (2017). Bufalin induces apoptosis in vitro and has Antitumor activity against human lung cancer xenografts in vivo. *Environmental Toxicology*, *32*(4), 1305–1317. https://doi.org/10.1002/tox.22325
38. Ye, Q., Lin, R., Chen, Z., Li, J., & Zheng, C. (2024). Isolation, Identification and Chemical Modification of Bufadienolides from Bufo melanostictus Schneider and Their Cytotoxic Activities against Prostate Cancer Cells. *Molecules*, *29*(7), 1571–1571. https://doi.org/10.3390/molecules29071571
39. Yeh, J., Huang, W. J., Kan, S., & Wang, P. S. (2003). Effects of bufalin and cinobufagin on the proliferation of androgen dependent and independent prostate cancer cells. *The Prostate*, *54*(2), 112–124. https://doi.org/10.1002/pros.10172

40. Yu, C., Kan, S., Pu, H., Jea Chien, E., & Wang, P. S. (2008). Apoptotic signaling in bufalin- and cinobufagin-treated androgen-dependent and -independent human prostate cancer cells. *Cancer Science*, *99*(12), 2467–2476. https://doi.org/10.1111/j.1349-7006.2008.00966.x
41. Zhang, Y., Dong, Y., Melkus, M. W., Yin, S., Tang, S.-N., Jiang, P., Pramanik, K., Wu, W., Kim, S., Ye, M., Hu, H., Lu, J., & Jiang, C. (2018). Role of P53-Senescence Induction in Suppression of LNCaP Prostate Cancer Growth by Cardiotonic Compound Bufalin. *Molecular Cancer Therapeutics*, *17*(11), 2341–2352. https://doi.org/10.1158/1535-7163.MCT-17-1296

Figures

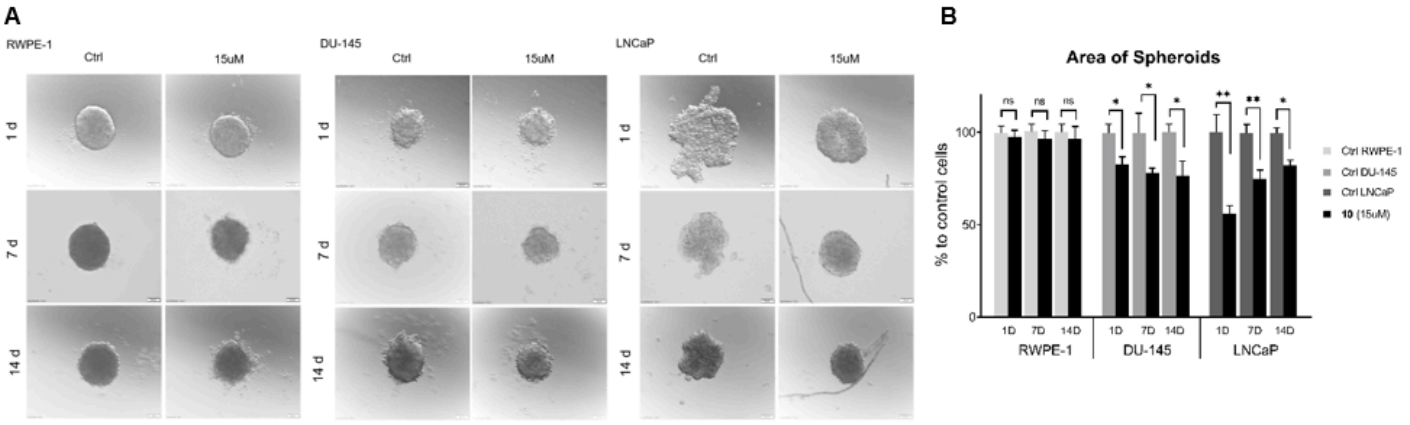

Figure 1

Time-dependent effect (1–14 days) of compound **10** (15 μM) on the cellular integrity of DU-145, LNCaP and RWPE-1 spheroids. (**A**) Representative images of untreated control and compound **10-**treated spheroids after 1, 7 and 14 days of treatment. Magnification, 100×. (**B**) Quantification of spheroid area using ImageJ. Data are expressed relative to untreated controls. Asterisks indicate significant differences compared with the corresponding control (*) $p < 0.05$, (**) $p < 0.01$. Representative images corresponding to all tested concentrations (2–25 μM) are shown in SI Fig. S3.

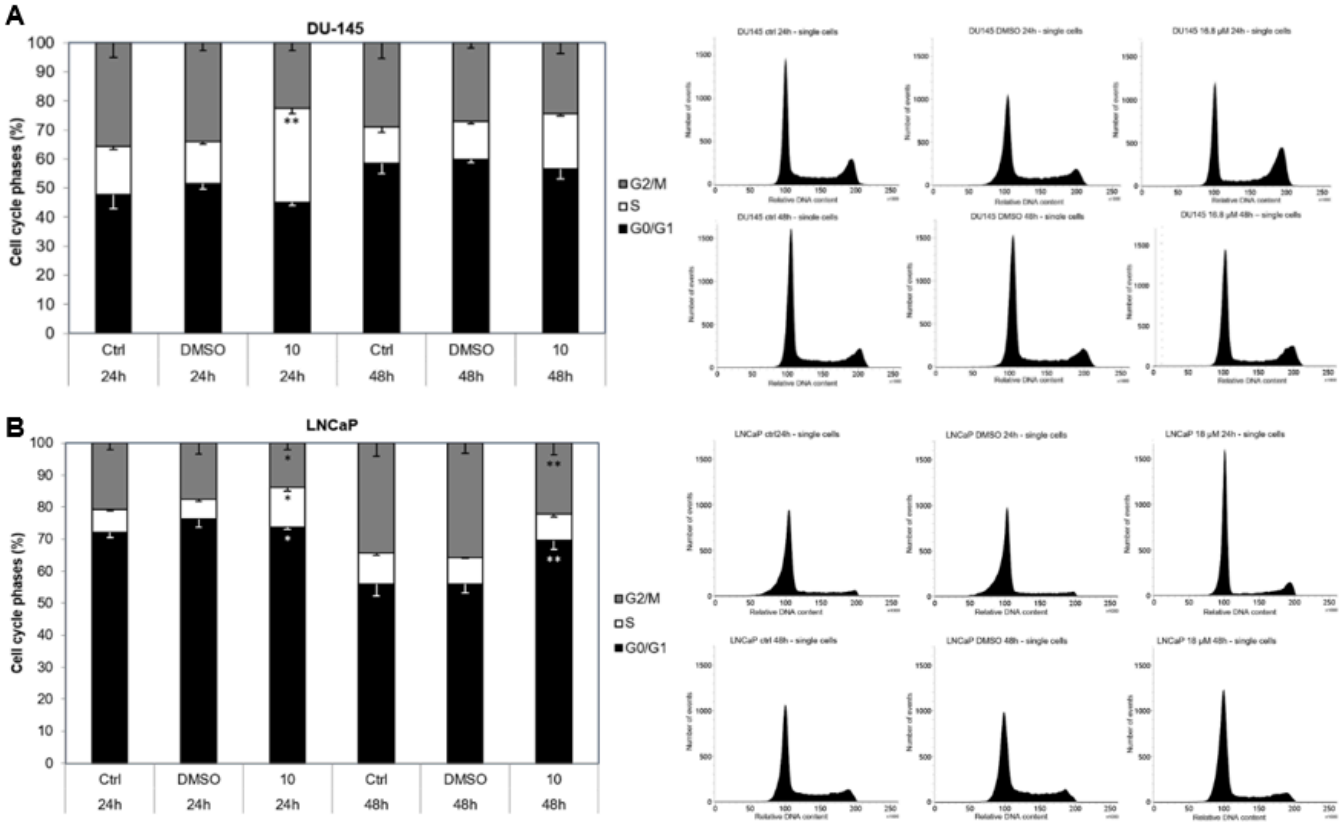

Figure 2

The effect of compound **10** on the cell cycle distribution in **(A)** DU-145 and **(B)** LNCaP cells. Percentages of cells in each cell of the cycle phase (G_1, S and G_2/M) are indicated. Asterisks denote values that are significantly different from control values at (*) $p < 0.05$, (**) $p < 0.01$.

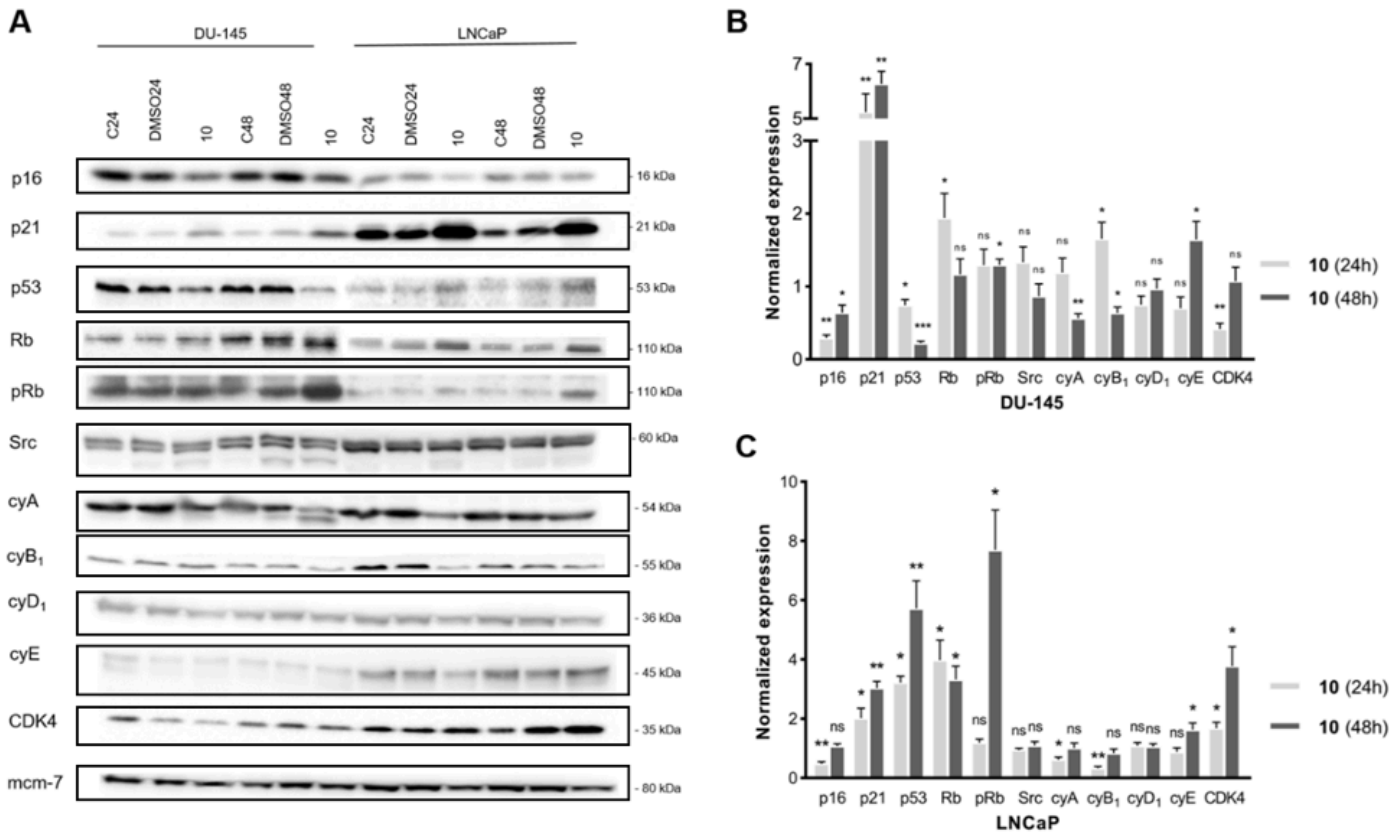

Figure 3

Effect of compound **10** on the expression of cell cycle regulatory proteins in DU-145 and LNCaP cells. (**A**) Representative Western blot analysis of cells treated with compound **10** at the IC_{50} concentration for 24 and 48 h compared with untreated controls (C24/C48). Quantification of protein expression in (**B**) DU-145 and (**C**) LNCaP cells. Protein expression was normalized to MCM-7 and expressed relative to the untreated control. Asterisks indicate significant differences compared with the corresponding control (*) $p < 0.05$; (**) $p < 0.01$; (***) $p < 0.001$.

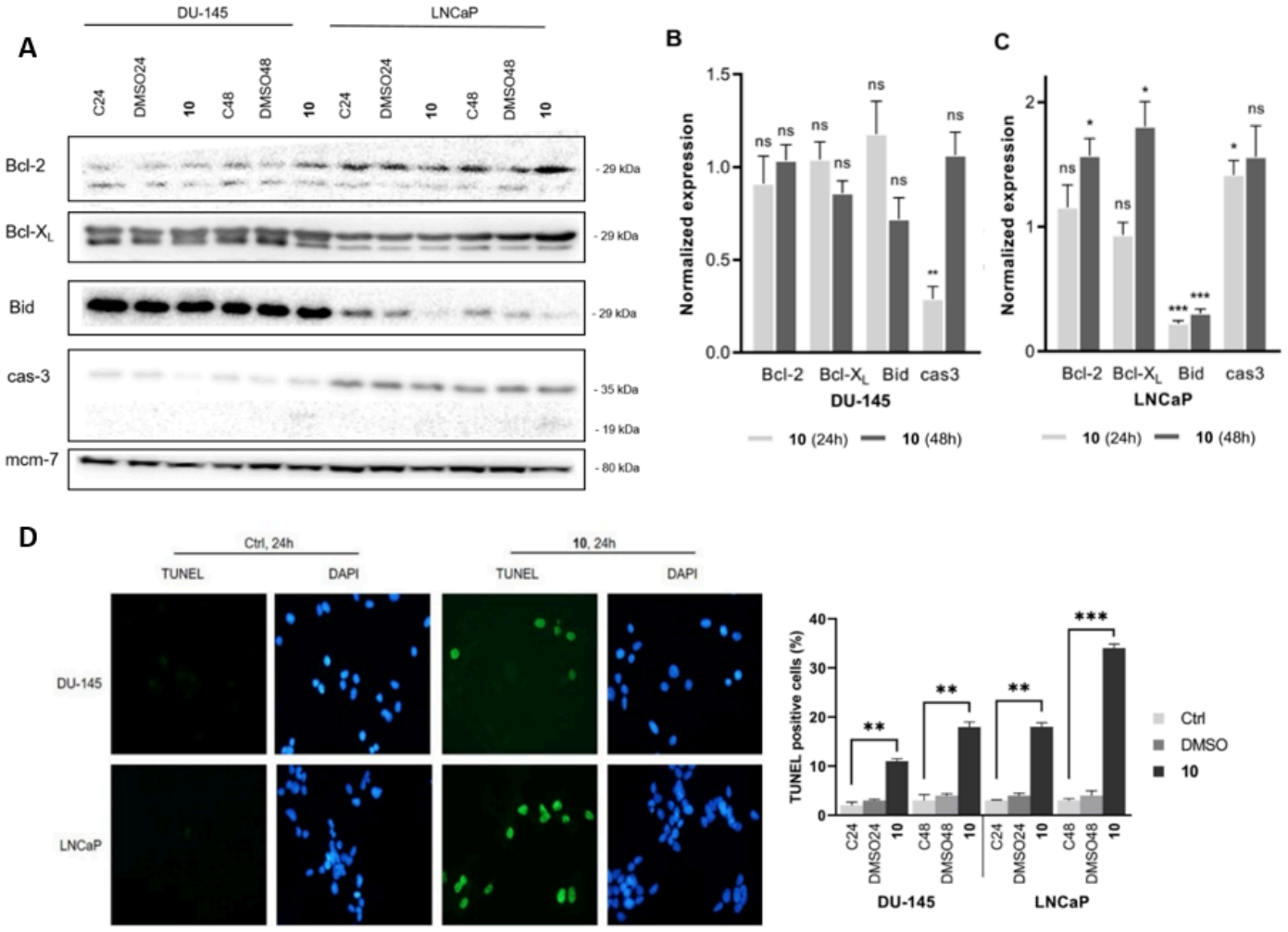

Figure 4

Effect of compound 10 on apoptosis in DU-145 and LNCaP cells. (**A**) Representative Western blot analysis of apoptosis-regulatory proteins in cells treated with compound **10** at the IC_{50} concentration for 24 and 48 h compared with untreated controls (C24/C48). Quantification of protein expression in (**B**) DU-145 and (**C**) LNCaP cells. Protein expression was normalized to MCM-7 and expressed relative to the untreated control. (**D**) Representative TUNEL staining of DU-145 and LNCaP cells treated with compound **10** at the IC_{50} concentration for 24 and 48 h. TUNEL-positive nuclei are shown in green and total nuclei (DAPI) in blue. Magnification, 400×. Data represent the mean ± SD of three independent experiments. Asterisks indicate significant differences compared with the corresponding control (*) $p < 0.05$; (**) $p < 0.01$; (***) $p < 0.001$.

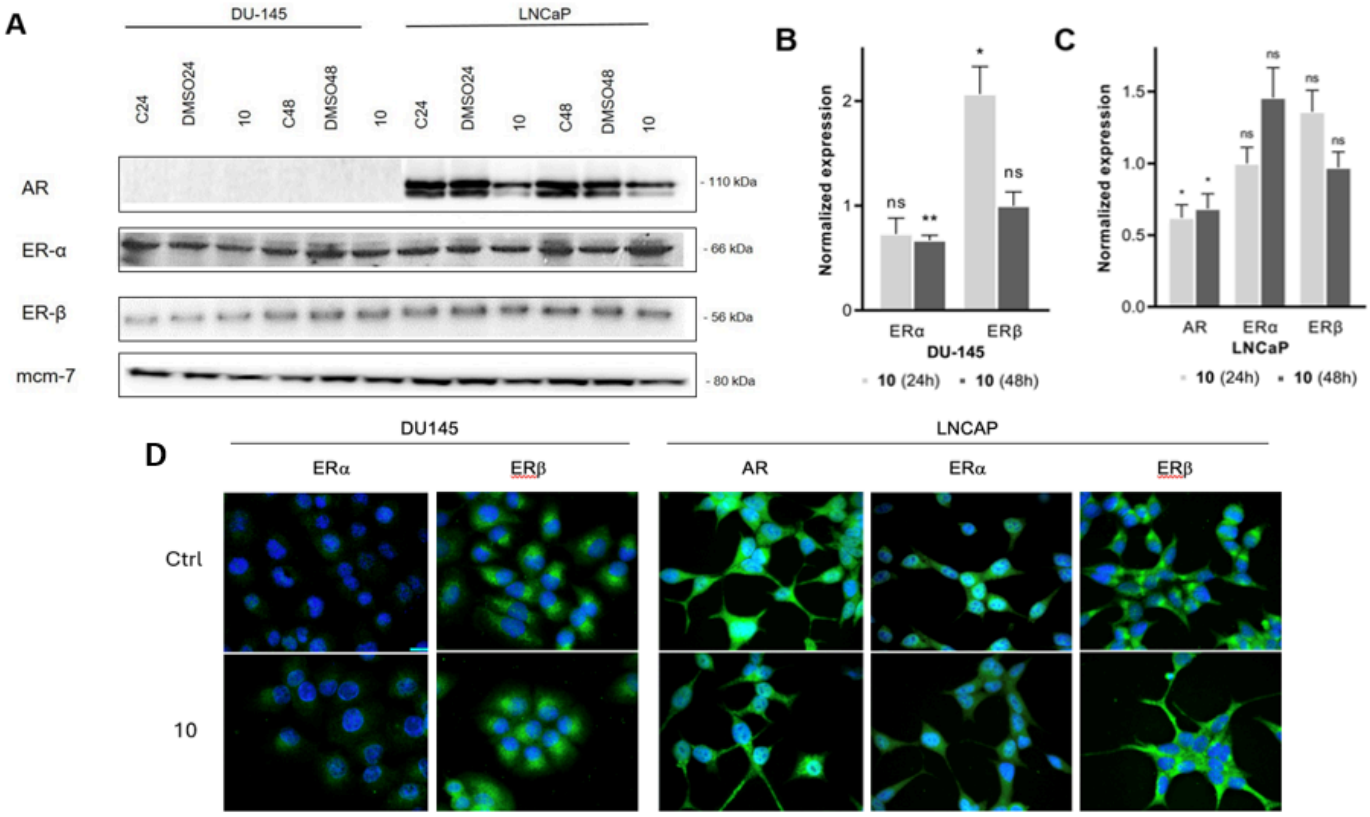

Figure 5

Effect of compound **10** on the expression of AR, ER-α and ER-β nuclear steroid receptors in DU-145 and LNCaP cells. (**A**) Representative Western blot analysis of cells treated with compound **10** at the IC_{50} concentration for 24 and 48 h compared with untreated controls (C24/C48). Quantification of protein expression in (**B**) DU-145 and (**C**) LNCaP cells. Protein expression was normalized to MCM-7 and expressed relative to the untreated control. Asterisks indicate significant differences compared with the corresponding control (*) $p < 0.05$; (**) $p < 0.01$; (***) $p < 0.001$. (**D**) Representative immunofluorescence images of AR, ER-α and ER-β in DU-145 and LNCaP cells treated with compound **10** at the IC_{50} concentration for 24 h. AR, ER-α and ER-β are shown in green and nuclei (DAPI) in blue. Complete images for each fluorescence channel are provided in SI Fig. S4. Magnification, 400×.

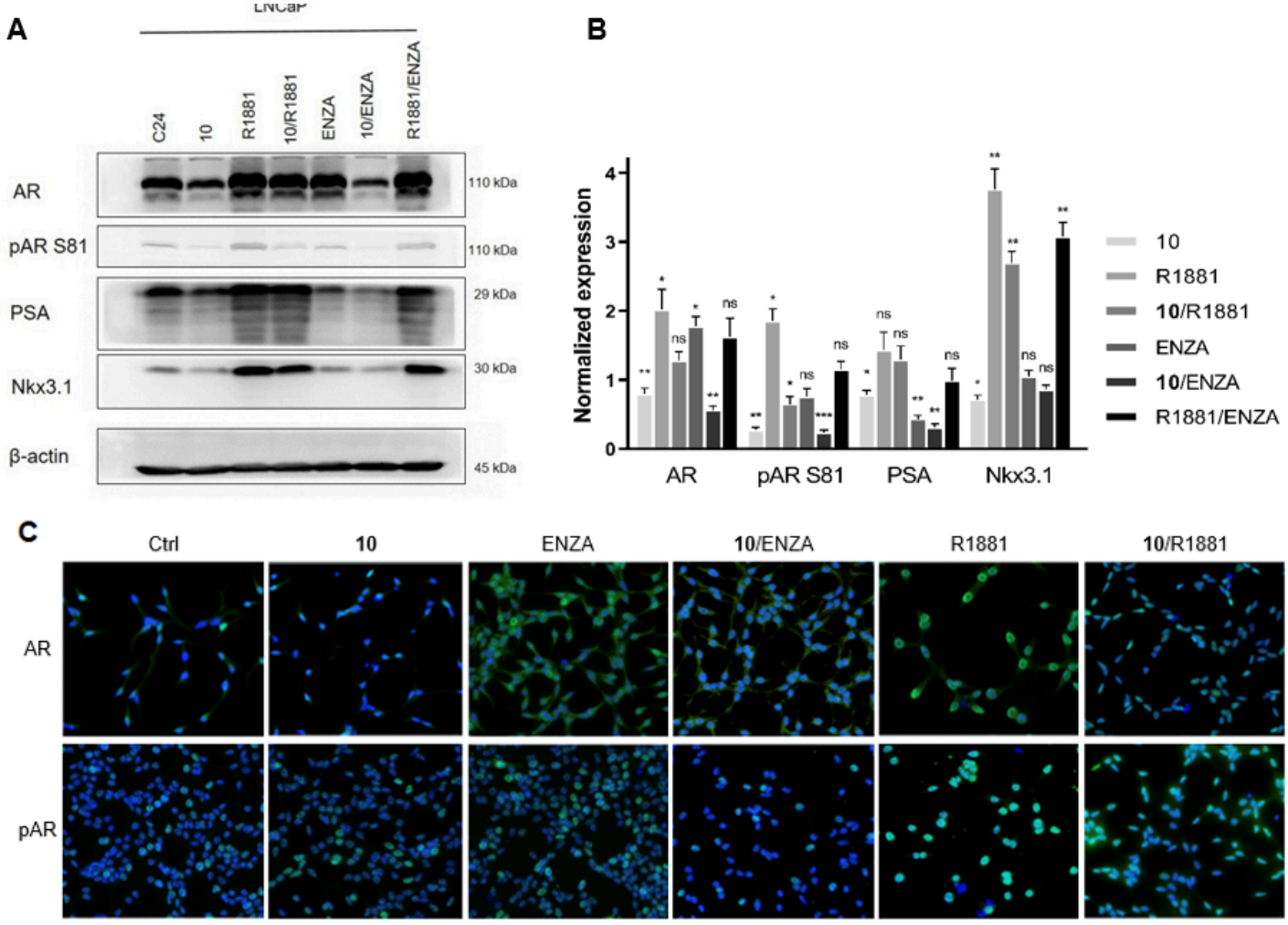

Figure 6

Effect of compound 10 on AR signalling in LNCaP cells. Analysis of AR-related proteins in LNCaP cells treated with compound **10** at the IC_{50} concentration, R1881 (1 nM), enzalutamide (1 μM), or their combinations for 24 h in charcoal-stripped serum medium, compared with untreated control (C24). (**A**) Representative Western blot. **(B**) Quantification of protein expression. Protein expression was normalized to β-actin and expressed relative to the untreated control. Asterisks indicate significant differences compared with the corresponding control (*) $p < 0.05$; (**) $p < 0.01$; (***) $p < 0.001$. (**C**) Representative immunofluorescence images of AR and phosphorylated AR (Ser81) in LNCaP cells treated under the same conditions. AR and pAR (Ser81) are shown in green and nuclei (DAPI) in blue. Complete images for each fluorescence channel are provided in SI Fig. S5. Magnification, 200×.

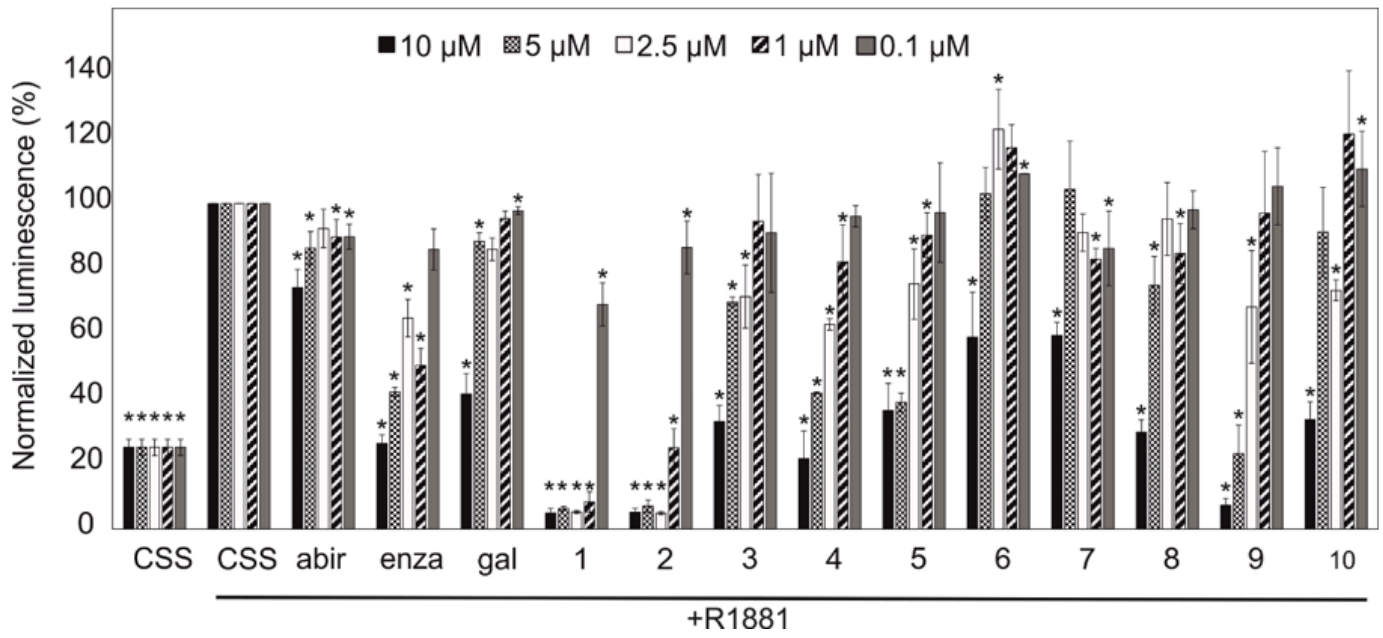

Figure 7

The influence of cardenolides and oleandrigenin-related androstane derivatives on the AR-mediated transcription in the 22Rv1-ARE14 reporter cell line for 24 h. Control cells were grown in charcoal-stripped serum medium (CSS). Cells were treated with 1 nM methyltrienolone R1881 or R1881 in combination with the tested compounds **1**-**10** in five different concentrations (10; 5; 2.5; 1; 0.1 µM) for 24 h in CSS. Abiraterone (abir), enzalutamide (enza) and galeterone (gal) were used as positive controls. The luciferase activity was measured in the cell lysate. The experiment was repeated at least three times in triplicates. The asterisks (*) designate statistically significant differences between control with 1 nM R1881 in CSS (CSS + R1881) and treated cells (p ≤ 0.05).

Supplementary Files

This is a list of supplementary files associated with this preprint. Click to download.

- Metzetal.SupplementaryInformationUncroppedWB.pdf
- Metzezal.SupplementaryInformation.pdf